POLITECNICO DI TORINO
Repository ISTITUZIONALE

Static and free-vibration analyses of dental prosthesis and atherosclerotic human artery by refined finite element models

Original
Static and free-vibration analyses of dental prosthesis and atherosclerotic human artery by refined finite element models / Carrera, E., Guarnera, D., Pagani, A.. - In: BIOMECHANICS AND MODELING IN MECHANOBIOLOGY. - ISSN 1617-7959. - 17:2(2018), pp. 301-317. [10.1007/s10237-017-0961-z]

Availability:
This version is available at: 11583/2704944 since: 2018-04-04T09:28:31Z

Publisher:
Springer Verlag

Published
DOI:10.1007/s10237-017-0961-z

Terms of use:

This article is made available under terms and conditions as specified in the corresponding bibliographic description in the repository

Publisher copyright
Springer postprint/Author's Accepted Manuscript

This version of the article has been accepted for publication, after peer review (when applicable) and is subject to Springer Nature's AM terms of use, but is not the Version of Record and does not reflect post-acceptance improvements, or any corrections. The Version of Record is available online at: http://dx.doi.org/10.1007/s10237-017-0961-z

(Article begins on next page)

15 November 2026

Static and free-vibration analyses of dental prosthesis and atherosclerotic human artery by refined finite element models

E. Carrera D. Guarnera A. Pagani

Mul^2, Department of Mechanical and Aerospace Engineering
Politecnico di Torino
Corso Duca degli Abruzzi 24, 10129 Torino, Italy

Static and modal responses of representative bio-mechanical structures are investigated in this paper by employing higher-order theories of structures and finite element approximations. Refined models are implemented in the domain of the Carrera Unified Formulation (CUF), according to which low- to high-order kinematics can be postulated as arbitrary and, eventually, hierarchical expansions of the generalized displacement unknowns. By using CUF along with the principle of virtual work, the governing equations are expressed in terms of fundamental nuclei of finite element arrays. The fundamental nuclei are invariant of the theory approximation order and can be opportunely employed to implement variable kinematics theories of bio-structures. In this work, static and free vibration analyses of an atherosclerotic plaque of a human artery and a dental prosthesis are discussed. The results from the proposed methodologies highlight a number of advantages of CUF models with respect to already established theories and commercial software tools. Namely, (i) CUF models can represent correctly the higher-order phenomena related to complex stress/strain field distributions and coupled mode shapes; (ii) bio-structures can be modelled in a component-wise sense by only employing the physical boundaries of the problem domain and without making any geometrical simplification. This latter aspect, in particular, can be currently accomplished only by using three-dimensional analysis, which may be computationally unbearable as complex bio-systems are considered.

1 Introduction

Biomechanics plays a fundamental role in modern science and research. The application of engineering tools in support of traditional medicine has been a success over the last decades. As an example, the advent of non-invasive, high-resolution imaging like ultrasounds or magnetic

resonance, together with the growth and the improvement of numerical modelling, filled the gaps of in vivo tests difficulties.

The human body is a complex grouping of different sub-systems, each of which with its own peculiarities and challenges from the modelling standpoint. Many works in the literature proposed mathematical models for compliant bio-structures. Some difficulties related to mechanical properties of soft tissues were analyzed in the pionering text by Fung [1]. The same author developed models to study the blood circulation and the growth of the bio-structures, see [2] and [3]. More recently, Evans [4] analyzed the whole muscle-skeletal apparatus and, subsequently, Hatze [5] proposed a set of control equations for the same system. In this context, it is possible to find outstanding studies about the dynamic modelling of bones (Frost [6]) and spine (Schultz [7]). Other works on the skeletal muscles focussed on the neural nature of the stimulus and the fibrous constitution. Famous examples are those who led to Hill's equation [8] and the introduction of the *cross-bridge* Huxley's theory [9]. Also, mathematical models of the heart were developed along the past decades to understand the complex behavior of this organ. The properties of cardiac fibers, for example, were studied in detail by Brady [10]. Many other authors, on the other hand, wrote about the mechanical behavior of the myocardium, see for example Edman and Nilsson [11] and Frank and Langer [12]. The same Fung, who is considered one of the precursor of bio-mechanics, dedicated some research and papers to this topic, presenting a mathematical formulation of the mechanical properties of the heart muscle based on the sliding-element theory, see [13].

This paper focuses on two problems that are sufficiently documented in the literature, i.e. the atherosclerotic plaque of a human artery and a dental implant. The atherosclerotic plaque is a vascular disease linked to lipid accumulation with progressive lumen reduction; the eventual plaque rupture may cause a thrombosis, which obstructs the blood flow leading to ischemia or heart infarctions (Sakakura *et al.* [14]). Some remedies to this problem exist eventually, see for example the balloon angioplasty (Holzapfel *et al.* [15]). Most of the knowledge about the argument and the recent advances are available also due to the numerous structural analyses conducted by researchers as mechanical tests (Lawlor *et al.* [16], Maher *et al.*[17]) as well as the materials characterization, see Holzapfel *et al.* [18] and Balzani *et al.* [19]. Because of the complexity of the problem and the advent of reliable numerical tools, structural models of the atherosclerotic plaque and many other bio-structures make use of the Finite Element Method (FEM). For instance, FEM was recently used for the axial characterization of the artery by Chai *et al.* [20] and for the evaluation of the circumferential stress within the artery bio-materials by Loree *et al.* [21]. Moreover, FEM was recently utilized to study patient-specific models of plaques, see Tang *et al.* [22].

Structural analysis of dental prostheses also acquired interest during the last decades. Those implants were introduced in the late 1960s and since then have been the object of many studies and publications. Most of the mechanical studies outlined how the interface between implant and bone is important (Geng *et al.* [23]), together with the exact evaluation of the loads. As discussed by Piliar *et al.* [24], in fact, an overload can lead to fatigue failure of the prosthesis.

On the other hand, Villancourt *et al.* [25] demonstrated that under-loading can cause atrophy. The geometry of the implant was investigated in detail by Dilek *et al.* [26] and Chiapasco *et al.* [27]. Recently, fatigue behavior was studied by Kayabasi *et al.*[28]. As for the atherosclerotic plaque, FEM is the most used method since Wider *et al.* [29] utilized it for dental implants in 1976. FEM was also employed to analyze the influence of materials features by Van Oosterwyck *et al.* [30] and to study the stress distribution in the tooth and within the bone.

Due to the complex geometry of bio-structures, most of the FEM models utilized in the literature and in common practice make use of three-dimensional (3D) brick elements based on elasticity. Although accurate they are, 3D finite elements are generally cumbersome from the point of view of computational costs. This issue is more emphasized as complex systems are considered, as for example in fluid-structure interaction analysis of biomedical applications. In this case, it is a common practise to couple 3D compliant models of a region of interest (e.g., an atherosclerotic plaque initiation within the cardiovascular system) with one-dimensional (1D) models describing the remaining zones, see Formaggia *et al.* [31]. In this context, the present paper aims at extending the use of higher-order 1D beam models with variable kinematics and enhanced accuracy to the analysis of biomedical structures for reducing the computational costs and avoiding complex coupling between physically inconsistent finite elements.

The mathematical models of the bio-structures discussed in this work are based on the Carrera Unified Formulation (CUF), which was first introduced in the field of mechanics of composite structures for plates and shells [32] and then extended to beams [33]. According to CUF, 1D and 2D theories of structures can be formulated with ease by expressing the displacement field as an arbitrary expansion of the generalized displacements. In this manner, the governing equations, eventually in the form of finite element arrays, can be written in terms of *fundamental nuclei*, see [34]. These nuclei are invariant of the theory approximation order and can be utilized to formulate generally refined models. In the domain of 1D CUF models, many progresses have been made in the last few years. For example, 1D CUF models have been successfully extended for the analysis of composite beams from macro/meso- [35] to micro-scale [36]; the component-wise analysis of aerospace [37] and civil engineering structures [38]; rotordynamics [39]; and multi-field analysis [40], among others. Interested readers can find more details about higher-order CUF beams and related applications in [41] along with a comprehensive review of classical as well as modern 1D models.

Preliminary results about the use of CUF for the analysis of compliant artery were discussed by Varello and Carrera [42], who utilized Taylor-like expansions of the three-dimensional displacement field for static response analyses. In the proposed work, on the other hand, refined beam models with component-wise capabilities are implemented by exploiting Lagrange expansions of the displacements on the cross-section domain. Thus, static and free vibration analyses of an atherosclerotic plaque and a dental implant are carried out. These Lagrange-based models highlight the possibility to describe local and complex stress/strain field distributions as well as the modal characteristics of the structures under consideration accurately. The paper is organized as follows: (1) first, CUF models are introduced as Taylor- and Lagrange-type

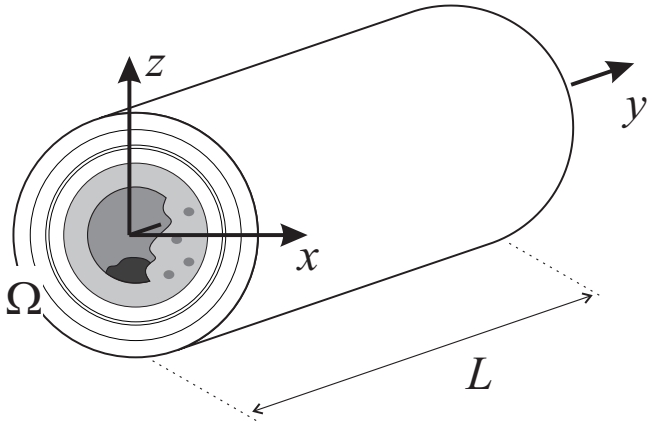

Figure 1: Generic beam structures and related reference system.

expansions of the generic kinematics field; (2) then, the component-wise approach is briefly outlined; (3) subsequently, the numerical results are detailed and discussed; and (4) finally, the main conclusions are drawn.

2 Unified beam theory with higher-order kinematics

Consider a generic cross-section beam structure as in Fig. 1. Referring to the given Cartesian coordinate system, the beam section Ω lays on xz-plane, whereas the length measures L along the y axis. The three-dimensional displacement vector is given in the following:

$$\mathbf{u}(x,y,z;t) = \left\{ \begin{array}{ccc} u_x & u_y & u_z \end{array} \right\}^{\mathrm{T}} \tag{1}$$

For the sake of completeness, the stress $\boldsymbol{\sigma}$ and strain $\boldsymbol{\epsilon}$ vectors are also introduced,

$$\boldsymbol{\sigma} = \left\{ \begin{array}{cccccc} \sigma_{xx} & \sigma_{yy} & \sigma_{zz} & \sigma_{xz} & \sigma_{yz} & \sigma_{xy} \end{array} \right\}^{\mathrm{T}}, \qquad \boldsymbol{\epsilon} = \left\{ \begin{array}{cccccc} \epsilon_{xx} & \epsilon_{yy} & \epsilon_{zz} & \epsilon_{xz} & \epsilon_{yz} & \epsilon_{xy} \end{array} \right\}^{\mathrm{T}}$$

Under the assumptions of small displacements and rotations, the strain components can be expressed in terms of displacements as:

$$\boldsymbol{\epsilon} = \boldsymbol{D}\boldsymbol{u} \tag{2}$$

where $\boldsymbol{D}$ is a linear differential matrix. On the other hand, in the case of linear elastic materials, stress and strain components are related each other by the Hooke's law,

$$\boldsymbol{\sigma} = \boldsymbol{C}\boldsymbol{\epsilon} \tag{3}$$

The components of matrices $\boldsymbol{D}$ and $\boldsymbol{C}$, which contains the material coefficients, are not given in this paper for brevity sake. However, interested readers can found them in Carrera *et al.* [34]. It is intended that, in the case of isotropic materials, as in the case of this paper, the material coefficients are functions of the elastic modulus E and the Poisson ratio ν.

2.1 Carrera Unified Formulation (CUF)

According to CUF, the kinematics of classical to higher-order beam theories can opportunely degenerate into a hierarchical expansion of the generalized unknowns $\mathbf{u}_\tau$, which are defined along the 1D domain; i.e.,

$$\mathbf{u}(x, y, z; t) = F_\tau(x, z)\mathbf{u}_\tau(y; t), \qquad \tau = 1, 2, \cdots, M \tag{4}$$

In Eq. (4), F_τ is a set of generic expansion functions over the cross-sectional domain and M stands for the number of terms employed in the displacement field. In the notation proposed, a repeated index denotes summation.

The choice of the functions F_τ and the parameter M determines the class and order (i.e., the accuracy and the computational costs) of the beam theory to be considered. Over the last few years, several expansions have been employed for the formulation of CUF-based 1D models, such as Taylor Expansions (TE), Lagrange Expansions (LE), Hierarchical Legendre Expansions (HLE), and any combinations of thereof in a variable-kinematics sense. The detailed description of these beam models is out of the scope of this paper. Interested readers can found further details in the literature, see for example [33, 43, 44] for TE, [45, 46] for LE, [47, 48] for HLE, and [49] for variable-kinematics theories. However, a brief discussion about TE and LE, which are the models employed in this paper for the analysis of bio-structures, are given hereinafter for completeness reasons.

One-dimensional TE models make use of McLaurin series polynomials $x^i z^j$ as F_τ cross-sectional functions, with i and j positive integers. As an example, the second-order ($N = 2$) TE beam model reads:

$$\begin{aligned}
u_x(x, y, z) &= u_{x_1}(y) + x\ u_{x_2}(y) + z\ u_{x_3}(y) + x^2\ u_{x_4}(y) + xz\ u_{x_5}(y) + z^2\ u_{x_6}(y) \\
u_y(x, y, z) &= u_{y_1}(y) + x\ u_{y_2}(y) + z\ u_{y_3}(y) + x^2\ u_{y_4}(y) + xz\ u_{y_5}(y) + z^2\ u_{y_6}(y) \\
u_z(x, y, z) &= u_{z_1}(y) + x\ u_{z_2}(y) + z\ u_{z_3}(y) + x^2\ u_{z_4}(y) + xz\ u_{z_5}(y) + z^2\ u_{z_6}(y)
\end{aligned} \tag{5}$$

In Eq. (5) the time parameter (t) is not shown for simplicity; this model has 18 generalized displacement variables/unknowns (displacements and derivatives). It is interested to note that classical beam models, such as Euler-Bernoulli Beam Theory (EBBT) and Timoshenko Beam Theory (TBT), are particular cases of the linear ($N = 1$) TE expansion, according to which $F_\tau = 1, x, z$.

In the case of heterogeneous structures, thin-walled or complex cross-sectional domains, the use of TE should be unsuggested. LE models make use of Lagrange polynomials sets as F_τ functions to unlocalize the displacement variables over a discrete cross-sectional domain, in a isoparametric sense. In the context of LE, beam theories with different orders can be implemented depending on the choice of the Lagrange polynomials set employed to describe the cross-sectional displacements. In fact, linear L3, bi-linear L4, or quadratic L9 beam theories can be implemented with ease by using CUF. As an example, the LE quadratic beam model

holds the following kinematics:

$$\begin{aligned} u_x(x,y,z) &= F_1\ u_{x_1}(y) + F_2\ u_{x_2}(y) + F_3\ u_{x_3}(y) + \cdots + F_9\ u_{x_9}(y) \\ u_y(x,y,z) &= F_1\ u_{y_1}(y) + F_2\ u_{y_2}(y) + F_3\ u_{y_3}(y) + \cdots + F_9\ u_{y_9}(y) \\ u_z(x,y,z) &= F_1\ u_{z_1}(y) + F_2\ u_{z_2}(y) + F_3\ u_{z_3}(y) + \cdots + F_9\ u_{z_9}(y) \end{aligned} \tag{6}$$

where $u_{x_1}, u_{x_2} \cdots, u_{z_9}$ are the primary mechanical variables of the problem and they are pure translational displacements. In this case, $F_1, \cdots, F_9$ are the following quadratic Lagrange polynomials:

$$\begin{aligned} F_\tau &= \tfrac{1}{4}(r^2 + r\ r_\tau)(s^2 + s\ s_\tau), \qquad \tau = 1,3,5,7 \\ F_\tau &= \tfrac{1}{2}s_\tau^2(s^2 + s\ s_\tau)(1-r^2) + \tfrac{1}{2}r_\tau^2(r^2 + r\ r_\tau)(1-s^2), \qquad \tau = 2,4,6,8 \\ F_\tau &= (1-r^2)(1-s^2), \qquad \tau = 9 \end{aligned} \tag{7}$$

where r and s vary above the cross-sectional natural plane between -1 and $+1$, and r_τ and s_τ represent the locations of the roots of the nine-node Lagrange polynomial set. According to LE modelling, higher-order beam theories can be opportunely formulated by increasing the polynomial order (e.g., cubic L16) or by using a combination of polynomial sets on the beam cross-section to have a piece-wise refined displacement field (see [45]).

2.2 Finite element formulation for free vibration and static analyses

Independently of the choice of the cross-sectional expanding functions F_τ, the Finite Element Method (FEM) can be employed to interpolate the generalized displacement variables along the beam axis. One has:

$$\mathbf{u}_\tau(y;t) = N_i(y)\mathbf{u}_{\tau i}(t), \qquad i = 1,2,\cdots,n \tag{8}$$

where $N_i(y)$ are the 1D shape functions (cubic four-noded Lagrange elements in this paper), n is the number of nodes of the finite element employed, and i denotes summation. $\mathbf{u}_{\tau i}$ is the vector of the nodal generalized displacements.

The equations of motion in the case of undamped free vibrations are obtained in terms of finite element arrays by using the principle of virtual displacements, which states that:

$$\delta L_{\text{int}} = -\delta L_{\text{ine}} \tag{9}$$

where L_{int} stands for the strain energy, L_{ine} is the work of the inertial loadings, and δ stands for the virtual variation. The virtual variation of the strain energy is rewritten by using Eqs. (2), (3), (4) and (8) to have:

$$\delta L_{\text{int}} = \int_V \delta\boldsymbol{\epsilon}^{\mathrm{T}}\boldsymbol{\sigma}\,\mathrm{d}V = \delta\mathbf{u}_{sj}^{\mathrm{T}}\mathbf{K}^{\tau sij}\mathbf{u}_{\tau i} \tag{10}$$

where $V = \Omega \times L$ is the volume of the beam and $\mathbf{K}^{\tau sij}$ is the stiffness matrix of the unified beam element in the form of 3×3 Fundamental Nucleus (FN). The derivation of the FN of the stiffness matrix is not repeated here for the sake of brevity, but it is given in [34]. However, the following terms of the stiffness nucleus are given for clarity purpose:

$$\begin{aligned} K_{xx}^{\tau sij} =& (\lambda + 2G) \int_L N_i N_j \mathrm{d}y \int_\Omega F_{\tau,x} F_{s,x} \mathrm{d}\Omega + G \int_L N_i N_j \mathrm{d}y \int_\Omega F_{\tau,z} F_{s,z} \mathrm{d}\Omega \\ &+ G \int_L N_{i,y} N_{j,y} \mathrm{d}y \int_\Omega F_\tau F_s \mathrm{d}\Omega \end{aligned} \tag{11}$$

$$K_{xy}^{\tau sij} = \lambda \int_L N_{i,y} N_{j,y} \mathrm{d}y \int_\Omega F_\tau F_{s,x} \mathrm{d}\Omega + G \int_L N_i N_j \mathrm{d}y \int_\Omega F_{\tau,x} F_s \mathrm{d}\Omega$$

where G and λ are the Lamé's parameters and comma denotes partial derivatives. If Poisson ν and Young E moduli are used, one has $G = \frac{E}{2(1+\nu)}$ and $\lambda = \frac{\nu E}{(1+\nu)(1-2\nu)}$. It can be demonstrated that all the components of $\mathbf{K}^{\tau sij}$ can be derived from Eq. (11) by permutations.

The fundamental nucleus of the mass matrix can be easily found by substituting CUF and FEM approximation into the expression of the virtual variation of the work of the inertial loadings; i.e.,

$$\begin{aligned} \delta L_{\text{ine}} &= \int_V \rho\, \delta \mathbf{u}^{\mathrm{T}} \ddot{\mathbf{u}}\, \mathrm{d}V \\ &= \delta \mathbf{u}_{sj}^{\mathrm{T}} \int_L N_i N_j \mathrm{d}y \int_\Omega \rho\, F_\tau F_s \mathrm{d}\Omega\, \ddot{\mathbf{u}}_{\tau i} = \delta \mathbf{u}_{sj}^{\mathrm{T}} \mathbf{M}^{\tau sij} \ddot{\mathbf{u}}_{\tau i} \end{aligned} \tag{12}$$

where ρ stands for the density of the material, and $\ddot{\mathbf{u}}$ is the acceleration vector. Given the F_τ CUF expansions and the shape functions N_i, the 3×3 mass and stiffness nuclei, $\mathbf{M}^{\tau sij}$ and $\mathbf{K}^{\tau sij}$, can be expanded versus the indexes $\tau, s = 1, \cdots, M$ and $i, j = 1, \cdots, n$ to obtain the elemental finite element arrays of the given refined beam element. Those matrices are thus assembled in the classical way of FEM for the description of the global problem. Also, by assuming harmonic displacements and according to Eq. (9), the free vibration analysis is reduced into a classical eigenvalue problem of the form:

$$(-\omega_k^2 \mathbf{M} + \mathbf{K}) \mathbf{u}_k = 0 \tag{13}$$

where $\mathbf{u}_k$ is the *k-th* eigenvector associated to the natural frequency ω_k.

In the case of linear static response analysis, the principle of virtual displacements holds

$$\delta L_{\text{int}} = \delta L_{\text{ext}} \tag{14}$$

where L_{ext} is the work of the external loadings. Upon substitution of CUF and FEM, the following algebraic system in the form of FN is obtained:

$$\mathbf{K}^{\tau sij} \mathbf{u}_{\tau i} = \mathbf{P}_{sj} \tag{15}$$

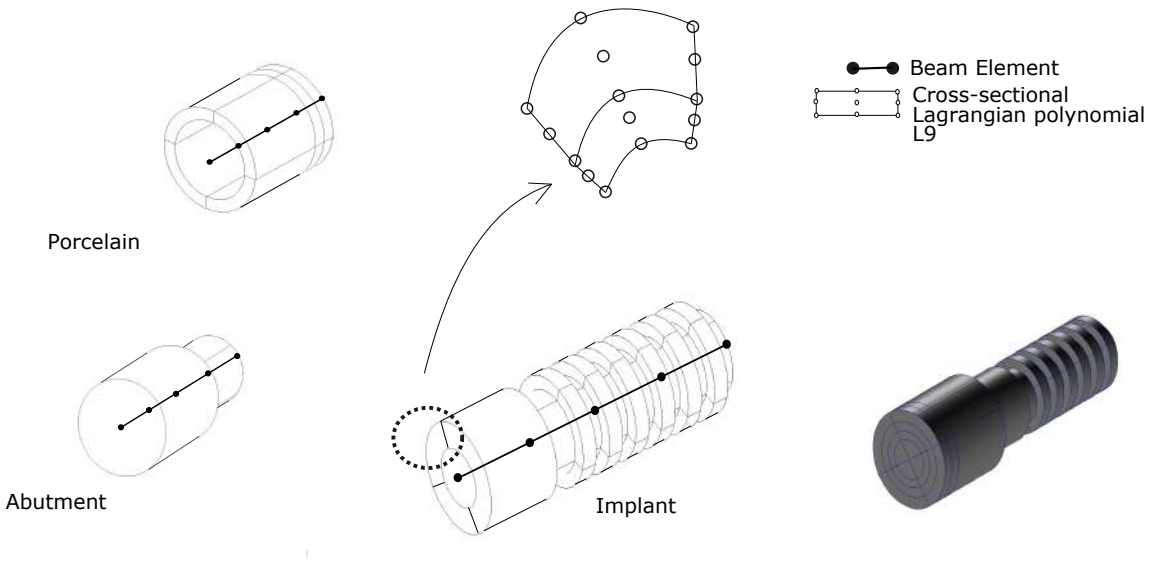

Figure 2: Component-Wise approach applied to biomedical structures.

In Eq. (15), $\mathbf{P}_{sj}$ represents the variationally coherent load vector, see [34]. Expanding Eq. (15) at element level by using aforementioned CUF index notation and assembling, the final algebraic system of equations can be inherently formulated and solved.

2.3 The Component-Wise approach

The analysis of multi-component structures is complex in common practice. These structures are made of different components, which are generally characterized by different scales and geometries in order to accomplish the technical and nature requisites. In the biomedical scenario, for example, skin, veins, arteries and capillaries as well as muscles are perfect examples of multi-component systems. Generally, the modelling of multi-component structures requires the adoption and the coupling of various mathematical models, even in the framework of finite element method. As a consequence, artificial techniques are usually involved to connect, for example, 1D, 2D and 3D finite elements that are kinematically inconsistent each other. This may result in numerical and physical uncertainties, especially if higher-order models are employed and in order to build sufficiently accurate models with reasonable computational resolution times.

In this domain, the enhanced capabilities of LE models, when coupled with FEM, are of particular interest for the analysis of multi-component structures. In recent works, in fact, it was demonstrated that LE-CUF models can be implemented in a *Component-Wise* (CW) sense to simulate complex structural assemblies in an efficient and geometrical/physical consistent manner, see [35, 50, 37, 51, 38]. As an example, Fig. 2 shows the CW approach as applied to a

Material	Young Modulus E, GPa	Poisson ratio ν
Ti-6Al-4V	110.00	0.32
Cobalt-Chromium alloy	220.00	0.30
Feldsphatic Porcelain	61.20	0.19
Gingiva	19.60×10^{-3}	0.30
Bone	14.70	0.30

Table 1: Mechanical properties of the materials used in the study of the dental implant.

dental prosthesis. According to CW, each component of the structure (i.e., implant, abutment, porcelain, etc.), is modelled by higher-order LE beam finite elements. These finite elements, by exploiting an LE approximation of the beam kinematics, make use of the physical surfaces for describing the problem domain. In this manner, the geometrical characterization of the structure is exact, and fictitious integration domains (e.g., beam axis in the case of classical 1D finite elements) are no more utilized. Moreover, because each component of the structure is modelled with the same kinematics, coupling is straightforward and no artificial mathematical links (e.g. multi-point constraints) are utilized.

The aforementioned properties of the CW modelling approach can be achieved, with the available technology, only if 3D finite elements are used. By using higher-order CUF, instead, enhanced geometrically-consistent models with low computational costs can be formulated inherently.

3 Numerical results

This section investigates the efficiency of the proposed formulation applied to the static and modal analyses of a dental implant and an atherosclerotic plaque. As different they are, these two analysis cases present some analogies, because they both are 1D problems in which one dimension is bigger than the cross-sectional dimensions. This aspect makes the dental implant and the atherosclerotic plaque significant to be studied by 1D higher-order models.

3.1 Dental implant

Dental prostheses have been largely investigated in several works over the last decades. These works primarily provided guidelines and design rules for resistant and long-duration prostheses, based on investigations about loading conditions and materials. This section, instead, will provide and assess, from the mechanical standpoint, innovative models for the static and free vibration analyses of this important bio-structure.

A cut-view of the addressed implant is shown in Fig. 3, where important dimensions are also given. The prosthesis is made of the materials whose properties are given in Table 1. Namely,

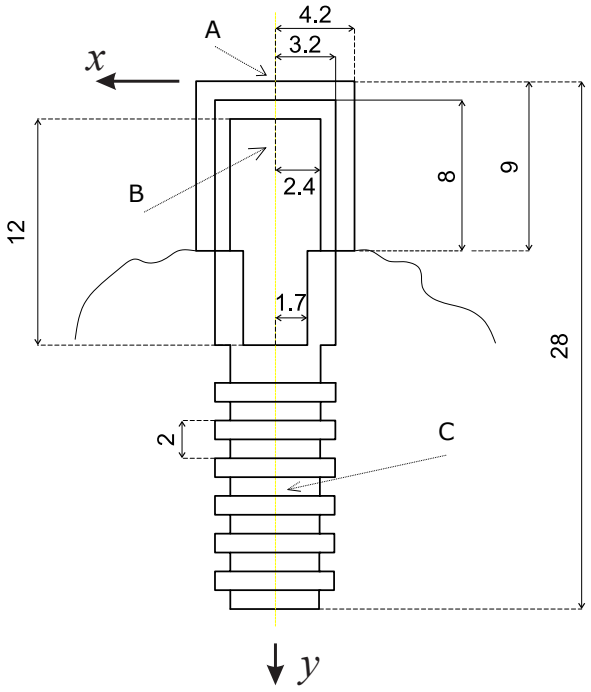

Figure 3: Dental implant. Dimensions in millimetres.

Ti-6Al-4V alloy is employed for implant fixture and abutment, cobalt-chromium alloy for metal framework and feldsphatic porcelain for occlusal material. Table 1 also gives the mechanical properties of the gingiva and bone, which are modelled in a second analysis case.

Figure 4 represents in detail the problem under consideration (whenever the implant, gingiva and bone are considered together) and the boundary conditions employed. In contrast, for static analyses, we consider, according to the literature, the bio-system undergoing a masticatory force of 118.2 N in the angle of approximately 75° to the occlusal plane, see Fig. 5.

In the following sections, classical, higher-order TE and LE beam models are implemented for static and free vibration analyses. In detail, Euler-Bernoulli Beam Theory (EBBT), Timoshenko Beam Theory (TBT) and up to the 16th-order refined TE models are considered. On the other hand, LE models that make use of piece-wise quadratic kinematics (L9 polynomials) on the beam cross-section are implemented in a CW sense. For all the CUF models, and if not differently specified, 24 four-noded 1D beam elements are used along the y-axis providing convergent solutions. CUF models are, thus, compared to 3D finite elements models implemented by using the commercial tool MSC.Nastran.

3.1.1 Static analysis

In the first analysis case, the tooth undergoes cantilever boundary condition (the base is fixed) and gingiva and bone are not considered. Table 2 shows the axial, u_y, and transverse, u_z,

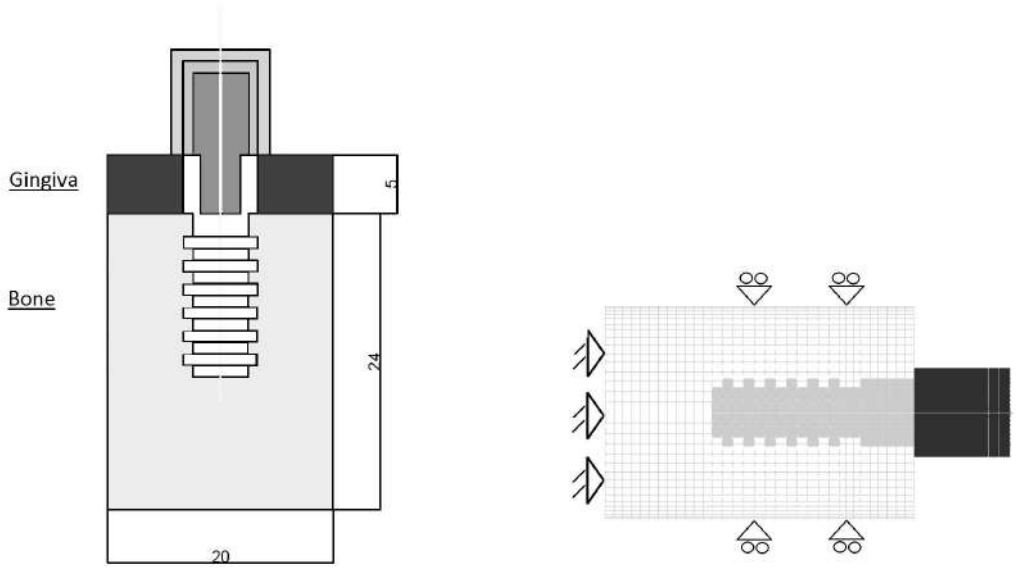

(a) (b)

Figure 4: Model of gingiva and bone (a) and representation of the boundary conditions (b).

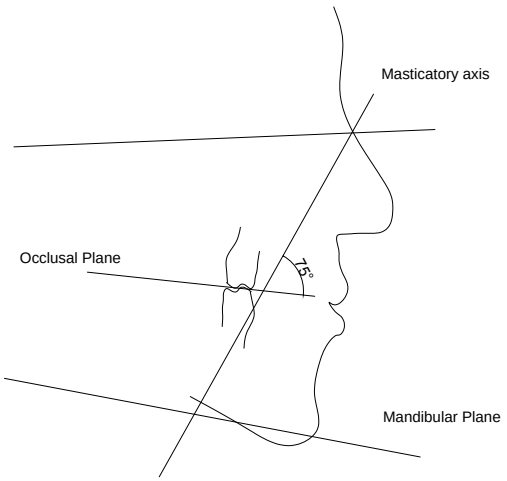

Figure 5: Direction of the masticatory force.

Model	$u_y^A \times 10^2$	$u_y^B \times 10^3$	$u_y^C \times 10^3$	$u_z^A \times 10^2$	$u_z^B \times 10^2$	$u_z^C \times 10^3$	DOFs
Classical beam models							
EBBT	-0.797	0.910	-0.590	-4.760	-3.892	-3.410	219
TBT	-0.797	0.910	-0.590	-4.825	-3.953	-3.590	365
Refined TE beam models							
N=1	-0.797	0.910	-0.590	-4.825	-3.953	-3.590	657
N=4	-0.978	1.010	-0.780	-5.827	-4.780	-4.190	3285
N=8	-1.016	1.030	-0.780	-6.045	-4.955	-4.330	9855
N=12	-1.027	1.030	-0.800	-6.134	-5.029	-4.390	19929
N=16	-1.035	1.040	-0.820	-6.172	-5.061	-4.410	33507
Component-wise LE models							
16LE	-1.442	1.040	-0.440	-6.219	-5.099	-4.430	9903
36LE	-1.028	1.030	-0.800	-6.127	-5.022	-4.370	26595
MSC.Nastran model							
Solid	-1.064	1.040	-0.830	-6.330	-5.190	-4.470	118368

Table 2: Displacements components (in mm) measured at three different points of the cantilever implant.

displacement components of the structure subjected the masticatory force. The results are given at different points over the problem domain and they are denoted with superscripts A, B, and C. Point A is placed at the loaded cross-section in correspondence of the loading point in the porcelain region; points B and C denote positions at $y = 3.75$ mm and $y = 22$ mm and they are placed in the metal framework and in the implant fixture, respectively (see Fig. 3). The table also gives the total number of degrees of freedom (DOFs) for each model considered. In this analysis, particular attention is given to the capability of the LE, which are obtained by using a CW piece-wise description of the kinematics by 16 and 36 L9 polynomials, and refined TE models to provide good results in terms of displacement components. This aspect is further underlined in Fig. 6, where the deformed configurations of the CW and the 3D FE models are compared. The accuracy of the proposed solutions is also discussed in terms of stress components. In detail, the compression and shear stresses, respectively σ_{yy} and σ_{yz}, at two different points over the structure domain (points B and C as discussed before) are measured and shown in Table 3. From these preliminary analyses it is clear that classical beam models and lower-order TE are not able to describe properly the displacement/stress states of the problem under consideration.

In the second analysis case of the investigation of the dental implant, the human jawbone, constituted by bone and gingiva, is considered as shown in Fig. 4. The loading condition remains unchanged with respect to the previous analysis case. However, in this case, only LE-CW models are considered in the domain of CUF models for two main reasons: i) LE provides

(a) CW model (b) MSC.Nastran Solid model

Figure 6: Deformed states of the cantilever implant subjected to the masticatory force.

Model	σ_{yy}^B	σ_{yy}^C	σ_{yz}^B	σ_{yz}^C
Classical beam models				
EBBT	-3.8742	-6.3379	-0.0010	-0.0016
TBT	-3.8742	-6.3379	-0.9647	-1.6027
Refined TE beam models				
N=1	-3.8742	-6.3379	-0.9647	-1.6027
N=4	-3.0357	-6.1978	-1.1452	-3.6212
N=8	-3.0178	-6.8915	-1.1334	-2.1038
Component-wise LE models				
36LE	-2.9558	-5.9619	-1.1363	-2.0221
MSC.Nastran model				
Solid	-3.0031	-7.0980	-1.1514	-2.2007

Table 3: Stress components (in MPa) measured at two different points of the cantilever implant.

Model	$u_y^D \times 10^4$	$u_y^E \times 10^4$	$u_y^F \times 10^4$	$u_z^D \times 10^3$	$u_z^E \times 10^4$	$u_z^F \times 10^6$	DOFs
52LE	-4.040	-6.440	-1.620	-4.372	-6.480	-9.028	51879
Solid	-4.050	-6.230	-1.630	-4.314	-6.070	-9.010	240900

Table 4: Displacements components (in mm) measured at three different points of the dental implant with gingiva and bone.

Model	σ_{yy}^D	$\sigma_{yy}^E \times 10^3$	σ_{yy}^F	σ_{yz}^D	$\sigma_{yz}^E \times 10^3$	$\sigma_{yz}^F \times 10^3$
52LE	-2.02	-2.01	-0.42	-0.59	-2.26	5.81
Solid	-1.97	-1.92	-0.42	-0.64	-2.19	5.46

Table 5: Stress components (in MPa) measured at three different points of the dental implant with gingiva and bone.

accurate description of the mechanics and geometry as complex problems are addressed; ii) it is possible to impose unconventional boundary conditions as LE expansions are used in the formulation of beam theories. Some results in terms of displacements are proposed in Table 4. Displacements are given at different locations over the problem domain. In particular, point D is placed in the titanium abutment at $y = 5.5$ mm; E refers to a position in the gingiva at $y = 11.5$ mm; and F is placed in the bone at $y = 30.5$ mm. Equivalently, at the same points, Table 5 shows representative stress values according to the CUF-based beam model and the 3D FEM model. For completeness reasons, the deformed configuration of the complete implant is shown in Fig. 7. Furthermore, Fig. 8 gives the cross-sectional distribution of the axial stress in correspondence to the bone region and at the structure mid-span, where the connection between the implant and the bone is clearly visible.

This preliminary analyses suggest the following comments:

- Higher-order TE as well as LE models are able to correctly describe both the stress/strain fields and the displacement behaviour of the dental prosthesis and in accordance with the 3D FE model.

- By using a non-local expansion of the problems unknowns by LE, in a CW sense, it is possible to model unconventional boundary conditions and complex anisotropy by using refined CUF models.

- The CW models are, thus, able to model efficiently, and with a minimum number of degrees of freedom, complex dental systems including prostheses, gingiva, and bone.

- The simulation of the whole system is of fundamental importance to take into account correctly the contribution of the boundary conditions in the mechanical behaviour of

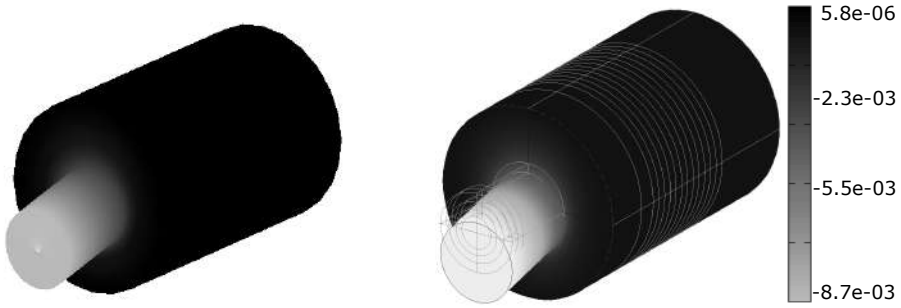

(a) CW model (b) MSC.Nastran Solid model

Figure 7: Deformed states of the dental implant with gingiva and bone.

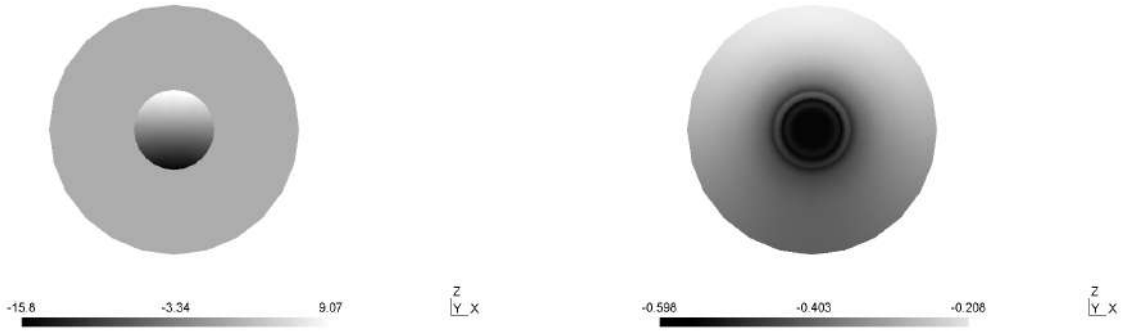

(a) $y = 11.5$ mm (b) $y = 30.5$ mm

Figure 8: Cross-sectional stress distribution (σ_{yy}, MPa) at the implant/bone (a) and bone (b) regions of the dental implant; CW model.

	Classical models		Refined TE			Component-wise LE		MSC.Nastran
Mode	EBBT	TBT	N=4	N=8	N=12	16LE	36LE	Solid
1	3965.15	3923.86	3568.11	3504.73	3478.72	3475.14	3481.85	3425.49
2	3965.15	3923.86	3568.11	3504.73	3478.74	3475.14	3481.85	3425.49
3	32433.55	29938.09	16410.06	16121.71	16047.48	16036.42	16029.23	16110.40
4	32433.55	29938.09	27761.70	27345.98	27205.19	27188.46	27213.56	27057.82
5	42529.07	42529.07	27761.71	27345.99	27205.19	27188.46	27213.57	27057.84
6	103394.59	85576.67	40171.04	39745.53	39588.58	39614.69	39609.81	39358.11
7	103394.59	85576.67	80168.17	79180.83	78856.99	78768.19	78795.07	78669.59
8	171762.92	148591.54	80168.20	79180.86	78857.01	78768.19	78795.38	78669.62
9	188578.58	148591.55	91871.75	90542.57	90221.70	90141.91	90100.98	90526.15
10	188578.59	171762.92	138344.74	136721.92	136164.44	135990.48	135974.07	135398.00
11	286659.60	216227.25	138344.78	136721.97	136164.49	135990.48	135976.33	135398.00
12	288447.87	216227.26	161735.77	160105.42	159683.80	159503.76	159446.00	159640.60
13	288447.88	283319.15	164241.16	162841.80	162352.75	162369.15	162322.57	162038.70
14	373792.71	283319.15	199983.86	197202.74	196317.07	196338.53	196177.06	195249.20
15	488979.41	286659.60	207556.83	204387.10	203717.14	196338.53	196185.05	195249.20

Table 6: Natural frequencies (Hz) of the cantilever dental implant (see Fig. 6).

the implant. The refined beam models represent a good candidate to replace current technology (3D FEM) for the enhanced analysis of this complex bio-structures.

3.1.2 Free vibration analysis

To further validate the proposed beam models and to fully characterize the dental implant under consideration, free vibration analysis is carried out and discussed in this section. Table 6 quotes the first 15 natural frequencies from classical to higher-order and CW models. The results, once again, are compared to those from a 3D finite element analysis. For the purpose of clarity, the same natural frequencies are shown in an histogram form in Fig. 9. Furthermore, some important mode shapes are depicted in Fig. 10. In detail, two flexural modes (Mode 1 and Mode 10) and two axial modes (Mode 3 and Mode 9) are depicted in this figure. Finally, in order to give a quantitative comparison in terms of mode shapes from the present CW beam models and 3D FEM analysis, the Modal Assurance Criterion (MAC) is employed and shown in Fig. 11 in the form of matrix and for the case under analysis. The MAC is defined as a scalar representing the degree of consistency (linearity) between one modal and another reference modal vector (see [52, 46]) as follows:

$$\mathrm{MAC}_{ij} = \frac{|\boldsymbol{\phi}_{A_i}^T \boldsymbol{\phi}_{B_j}|^2}{\boldsymbol{\phi}_{A_i}^T \boldsymbol{\phi}_{A_i} \boldsymbol{\phi}_{B_j} \boldsymbol{\phi}_{B_j}^T} \tag{16}$$

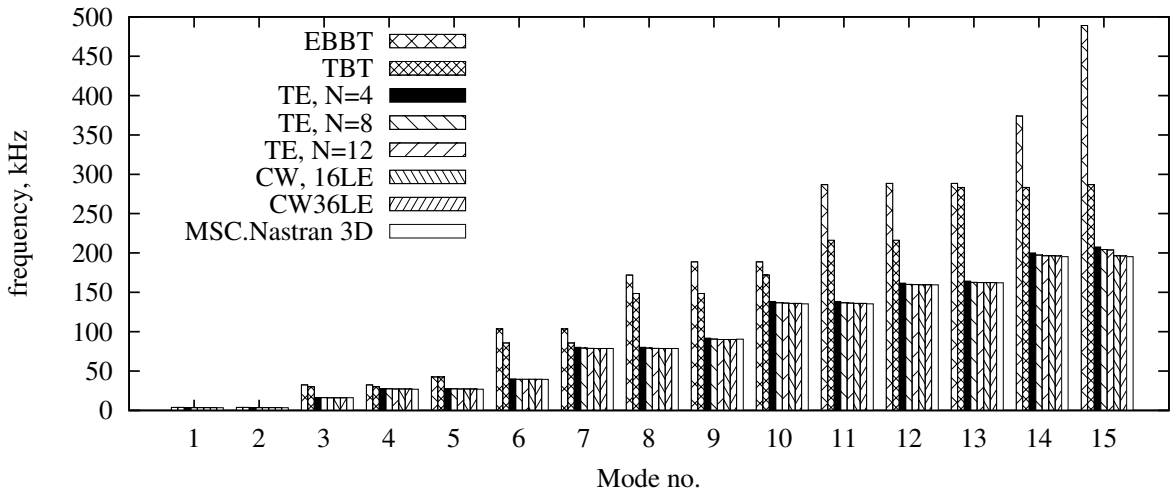

Figure 9: Natural frequencies of the dental implant vs. numerical model adopted.

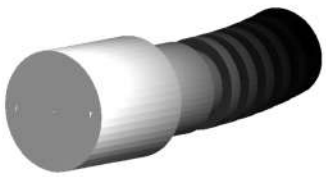

(a) Mode 1

(b) Mode 3

(c) Mode 9

(d) Mode 10

Figure 10: Representative mode shapes of the dental implant; CW model.

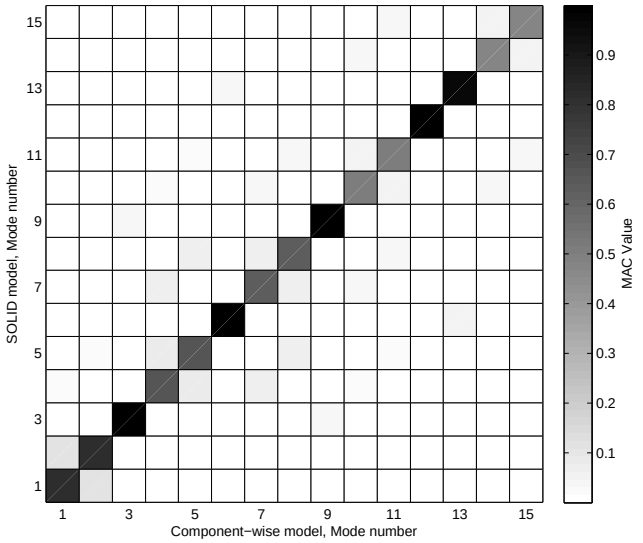

Figure 11: MAC matrix of the eigenvectors from traditional 3D FEM solution and 36LE CW model.

where $\boldsymbol{\phi}_{A_i}$ is the i^{th} eigenvector of model A, whereas $\boldsymbol{\phi}_{B_j}$ is the j^{th} eigenvector of model B. The modal assurance criterion takes on values from zero (representing no consistent correspondence), to one (representing a consistent correspondence).

The following comments arise from the modal analysis of the dental prosthesis:

- Classical beam models, EBBM and TBT, are able to describe correctly the first bending mode. Nevertheless, as shown in Fig. 9, they provide increasing inaccurate results as higher frequencies are considered.
- Conversely, refined TE and CW CUF-based beam models can describe very accurately the modal characteristics of the dental implant and in accordance with more complex 3D solid models made of brick elements.
- In detail, as confirmed by the MAC analysis (Fig. 11), CW models present a enhanced accuracy with respect to other beam models and in accordance to 3D analysis even in terms of consistency of the mode shapes. In fact, it is clear that the mode shapes from the CW model are perfectly equivalent to those from the solid model.

3.2 Atherosclerotic plaque

Another compelling case that demonstrates the capabilities of 1D-CUF models is the one concerning the human external iliac artery with a pronounced atherosclerotic plaque. In particular, a portion of an atherosclerotic artery with a significant lumen reduction is taken into account

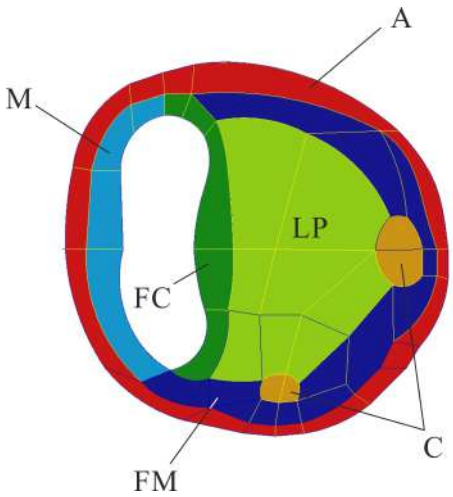

Figure 12: Cross-section of the atherosclerotic plaque.

in this section. Published literature shows that, starting from images captured during hrMRI (high resolution magnetic resonance imaging) and from histological analysis, it is possible to identify the section with its components [18, 19]. In this way, one can distinguish six different materials for the artery (see Fig. 12): the adventititia (A), the calcification (C), the lipid pool (LP), the fibrous cap (FC), the non-diseased media (M), and the fibrotic media (FM), which is in fact the sum of fibrotic intima and diseased fibrotic media.

For representative purpose, the cross-section width of the problem considered hereinafter is approximately 15 mm, as well as the height. As in the previous example, we present two different cases of boundary conditions and loads. The first one considers a portion of an artery with a length of 40 mm, clamped at the beam ends ($y = 0$ and $y = L$) and subjected to an internal pressure of 180 mmHg. In the second analysis case, an axial asymmetric load is applied and clamped-free boundary conditions are imposed to investigate the bending behaviour of the structure. Three-dimensional solid models are implemented in MSC.Nastran to conduct comparisons. These models are discretized with 382700 brick elements (398041 nodes) to give 1194123 DOFs. In this section high-order CUF models, TE and LE, are employed as well. In this case, the structure is modelled with a one-dimensional mesh made of 10 B4 (cubic) finite elements and an increasing value of beam theory orders are considered. The LE model's cross-section are, instead, discretized with 59 L9 and two L6 polynomials, for a total of 270 nodes. For the sake of completeness, the LE model discretization on the cross-section is shown in Fig. 13. Tissue materials are modelled as linear isotropic; the isotropic properties of each materials are the same as used in [18, 42] and are given in Table 7.

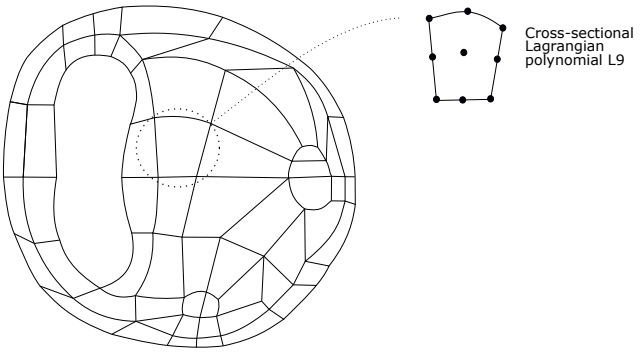

Figure 13: LE model of the atherosclerotic plaque.

Tissue	E [MPa]	ν
Calcification	12	0.33
Lipid Pool	0.1	0.33
Fibrous Cap	2.4	0.33
Media	1	0.33
Fibrotic Media	5	0.33
Adventitia	2.5	0.33

Table 7: Materials properties of the atherosclerotic plaque.

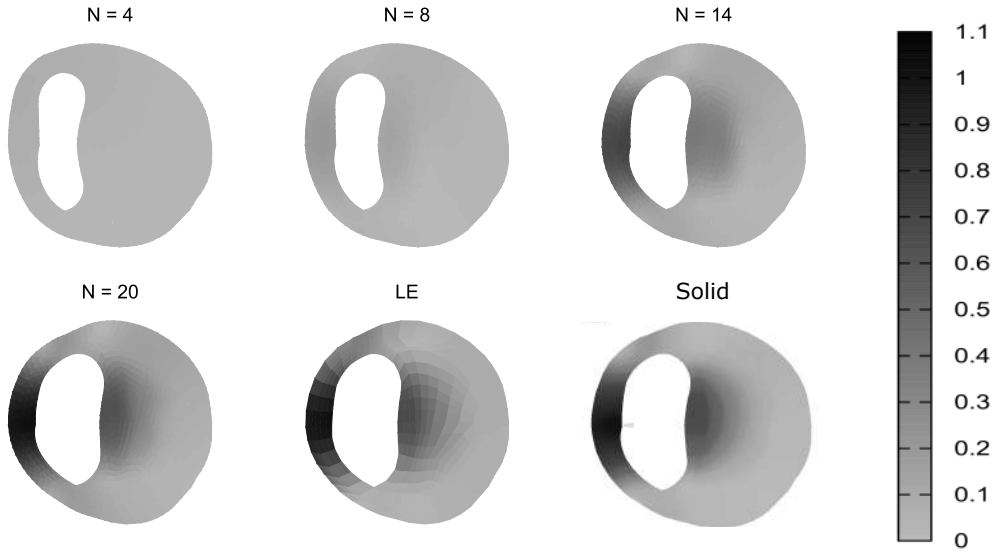

Figure 14: Distribution of the in-plane horizontal displacement component, u_x, on the mid-span cross-section. Comparison between TE ($N = 4$ to $N = 20$), LE, and MSC.Nastran Solid model. Values in mm.

3.2.1 Static Analysis

The complexity of the problem is confirmed, in the case of the first loading scenario, by Fig. 14, which shows the cross-sectional displacements distribution for various CUF beam models and 3D analysis. The thought heterogeneity of the atherosclerotic plaque is well described by the refined models proposed, which highlight the deformability of the lipid pool and the fibrous cap. In contrast, it is clear that the deformation in the calcification region is almost null. It is obvious that, to detect high cross-section deformation with beam theories, refined kinematics are needed but, still, 3D solution may be obtained. To confirm this aspect, Table 8 quotes the maximum displacements within the media (M), the adventitia (A) and the fibrous cap (FC) for the different models addressed. Furthermore, the total numbers of DOFs for each model employed are shown in the same table. Table 9, on the other hand, lists static analysis results in terms of stress components according to all models considered. Namely, the in-plane normal stress component, σ_{xx}, and the shear, σ_{xz}, are given in Table 9 and measured at different points in the atherosclerotic plaque domain. Some comments arise from the results outlined above:

Model	u^M_{max}	u^A_{max}	u^{FC}_{max}	DOFs
EBBT	0.0041	0.0041	0.0041	93
TBT	0.0093	0.0093	0.0093	155
N=1	0.5666	0.6210	0.3496	279
N=4	0.0538	0.0539	0.0262	1395
N=8	0.2019	0.1933	0.1232	4185
N=10	0.3088	0.2877	0.1710	6138
N=14	0.7065	0.6662	0.3862	11160
N=18	0.9213	0.8929	0.5552	17670
N=20	1.0294	1.0035	0.6211	21483
LE	1.0153	0.9581	0.7209	26730
Solid	1.0587	1.0488	0.7209	1194123

Table 8: Maximum horizontal displacement component, u_x (mm), of the atherosclerotic plaque subjected to internal pressure.

Model	σ_{xx}	σ_{xz}	σ_{xx}	σ_{xz}	σ_{xx}	σ_{xz}	σ_{xx}	σ_{xz}	σ_{xx}	σ_{xz}	σ_{xx}	σ_{xz}
	FM		M		LP		A		FC		C	
N=4	2.683	0.101	1.379	0.000	0.011	0.000	-0.010	-0.225	3.984	0.045	1.077	1.522
N=8	0.279	-0.011	2.772	-0.185	-0.280	0.017	2.012	0.032	1.658	0.259	-2.607	1.252
N=10	-6.965	-0.203	-1.788	-0.181	0.164	0.059	1.720	-0.683	-1.120	0.088	2.866	0.379
N=14	-2.345	-0.057	-9.435	-0.098	-2.066	0.070	2.534	-1.726	-9.756	-0.408	1.936	0.709
N=18	-1.382	-0.232	-9.188	-0.160	-0.857	0.120	5.820	-1.441	-5.981	-0.482	3.985	-0.708
N=20	1.132	0.140	-4.668	-0.187	-1.150	0.118	4.870	-1.919	-4.424	-0.276	6.786	-1.332
LE	-0.052	-0.025	-3.670	-0.546	-1.310	0.105	4.550	-1.750	-5.290	0.072	3.370	0.920
Solid	-0.186	-0.014	-1.907	-0.246	-1.458	0.137	4.649	-1.635	-1.926	0.119	3.206	0.860

Table 9: In-plane normal, σ_{xx}, and shear, σ_{xz}, stress components (10^2 MPa) in correspondence of each different material of the atherosclerotic plaque subjected to internal pressure.

(a) $N = 20$ (b) LE (c) Solid

Figure 15: Axial stress σ_{yy} (MPa) distribution on the mid-span cross-section of the atherosclerotic plaque subjected to clamped-free boundary conditions and forces along y.

Model	σ_{yy} at (0,0)	σ_{yy} at (15,0)	u_{max}^{M}	u_{max}^{FC}
EBBT	0.345	-0.090	12.574	12.574
TBT	0.345	-0.090	12.574	12.574
N=1	0.345	-0.090	12.574	12.574
N=4	0.322	-0.098	12.117	12.113
N=8	0.345	-0.089	11.983	12.149
N=10	0.331	-0.094	11.795	11.992
N=14	0.333	-0.084	11.447	11.848
N=18	0.327	-0.086	11.339	11.865
N=20	0.353	-0.088	11.304	11.862
LE	0.324	-0.080	11.245	11.704
Solid	0.340	-0.087	10.955	11.707

Table 10: Values of σ_{yy} (MPa) and u_x (mm) for different points and materials of the section.

- Classical and low-order TE models are not able to identify correct values of stress and displacements.
- Increasing the order of TE CUF models, it is possible to meet the accuracy of 3D analyses.
- LE model is able to reproduce the 3D solution with very low computational cost.

In a second load case, the structure is subjected to clamped-free boundary conditions. An asymmetric and axial pressure distribution is applied all along the lipid pool and the non-diseased media to simulate bending due to viscous forces along the y-axis. Accordingly, Figure 15 shows the distribution of the σ_{yy} axial stress components over the cross-section of the atherosclerotic plaque. Moreover, the same stress component is listed in Table 10 for various points and along with maximum horizontal displacements. The following considerations can be made:

Mode	Solid	LE	EBBT	TBT	N=1	N=4	N=8	N=10
1	133.63	134.12	246.26	170.22	164.04	155.92	141.34	139.44
2	138.06	138.85	259.15	174.24	170.15	147.86	146.53	144.32
3	235.41	236.73	-	-	251.93	249.43	244.67	243.45
4	247.65	258.78	-	-	-	-	-	331.14
5	256.51	258.83	598.93	349.94	339.49	316.54	285.33	278.51
6	270.22	272.26	633.59	361.64	351.67	301.34	295.71	290.05
7	309.85	310.97	-	-	373.61	368.84	356.66	349.72
8	311.76	325.77	-	-	-	-	-	-
9	319.54	329.08	-	-	-	611.04	478.45	462.58
10	340.83	348.22	-	-	-	-	-	-
11	342.64	354.95	-	-	-	617.55	501.94	478.91
12	385.71	390.33	-	-	-	644.86	434.66	414.72
13	387.44	396.67	-	-	-	-	-	-
14	393.04	397.51	-	-		-	-	-
15	400.98	409.27	-	-	-	-	585.31	547.56
16	425.57	440.64	-	-	-	-	-	-
17	432.91	438.87	-	-	-	493.22	478.35	478.92
18	434.25	443.75	-	-	-	711.92	566.41	510.85
19	441.07	451.96	-	-	-	-	-	-
20	442.76	448.23	-	-	-	-	-	535.37

Table 11: Natural frequencies (Hz) of the clamped-clamped atherosclerotic plaque.

- Classical and lower-order beam models, due to their intrinsic hypotheses, cannot detect different values of displacement for different materials over the cross section.
- In the case of bending loading, refined CUF models are very reliable and in accordance to 3D analysis. Moreover, the efficiency of these models is demonstrated as well.

3.2.2 Free-Vibration Analysis

The free-vibration analysis of the artery under clamped-clamped boundary conditions is presented as a final analysis case. The first 20 natural frequencies are shown in Table 11, where the solutions from the proposed 1D models are compared to those from 3D FE analyses. For representative reasons, selected mode shapes by 1D LE-CW model are also depicted in Fig. 16. Finally, the MAC matrix between the present CW model and the 3D brick model is shown in 17, to further highlight the congruence of the analysis. According to those results, the following remarks can be outlined:

- Classical and lower-order TE models can detect bending modes. Obviously, these 1D models cannot deal with mode shapes that involve cross-section deformations.
- In contrast, the LE-CW model can perfectly reproduce 3D accuracy in terms of both

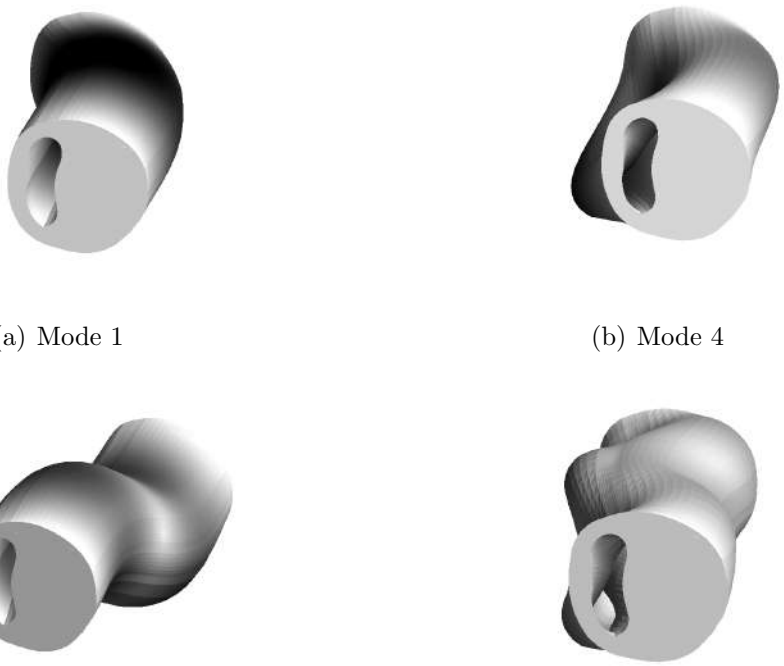

(a) Mode 1

(b) Mode 4

(c) Mode 6

(d) Mode 18

Figure 16: Representative mode shapes of the atherosclerotic plaque; CW model.

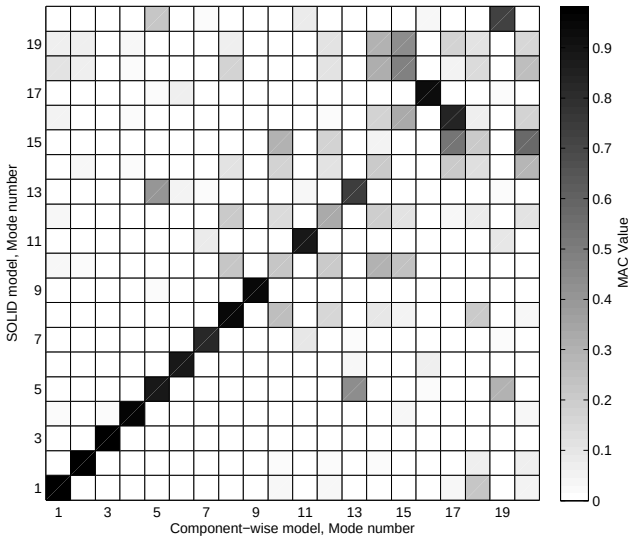

Figure 17: Modal Assurance Criterion (MAC) between 3D FEM solution and LE model.

natural frequencies and vibration modes. Some small discrepancies of mode shapes are noticed in high-frequency range, but this is justified by the enormous computational efficiency of CUF versus 3D solution.

4 Conclusions

Static and free-vibration analyses of a dental prosthesis and an atherosclerotic human artery have been investigated in this paper by using refined beam models. The adopted theories have been derived from the Carrera Unified Formulation (CUF), which allows to obtain a generic order beam theory in a compact and automatic way. Particular attention has been focused on the capability of LE (Lagrange Expansion) models based on CUF to represent in an accurate manner both the physical geometry and the kinematics of the problems under consideration in an accurate manner. All the results discussed have been compared to those from the literature and those obtained by using commercial finite element software tools. Some conclusions can be summarized:

- Refined models are necessaries to deal with complex bio-structures and arbitrary geometries.
- Component-wise approach based on LE helps us to overcome the necessity to combine different kinematics (1D, 2D, and 3D) to analyze multi-component and heterogeneous structures.
- The use of classical and lower-order beam models should be unsuggested for this class of problems. Using low-order kinematics, even in a global-local sense, and in regions where accurate analysis is not needed, may in fact result into wrong description of boundary conditions and error growing in local zones that are described by enriched kinematics.
- 1D CUF models have be demonstrated to eventually present high level of accuracy with low computational effort, when compared to 3D FEM models.

The results discussed encourage future use of the proposed models to more complex applications including, for instance, non-linear material laws and fluid-structure couplings.

Conflict of interest

No potential conflict of interest is reported by the authors.

References

[1] Y.C. Fung. *Biomechanics: Mechanical Properties of Living Tissues*. Springer, 1993.

[2] Y.C. Fung. *Biomechanics: Circulation*. Springer, 1997.

[3] Y.C. Fung. *Biomechanics: Motion, Flow, Stress and Growth*. Springer, 1990.

[4] F.G. Evans. *Biomechanical studies of musculo-skeletal system*. Charles C. Thomas, 1961.

[5] H. Hatze. A complete set of control equations for the human musculo-skeletal system. *Journal of Biomechanics*, 10:799–805, 1977.

[6] H.M. Frost. *Bone Remodelling Dynamics*. Charles C. Thomas, 1963.

[7] A.B. Schultz. Loads on the human lumbar spine. *Mechanical Engineering*, 108:36–41, 1986.

[8] A.V. Hill. The heat of shortening and the dynamic constants of muscle. *Proceedings of the Royal Society of London*, 126:136–195, 1938.

[9] H.E. Huxley and J. Hanson. Changes in the cross-striations of muscle during contraction and stretch and their structural interpretation. *Nature*, 173:973–976, 1954.

[10] A. Brady. Mechanical properties of cardiac fibers. In R.M. Berne, N. Sperelakis, and S.R. Geiger, editors, *Handbook of Physiology. Sec. 2, The Cardiovascular System*, volume 1, pages 461–474. American Physiology Society, 1979.

[11] K.A.P. Edman and E. Nilsson. The mechanical parameters of myocardial contraction studied at a constant length of the contractile element. *Acta Physiologica*, 72:205–219, 1968.

[12] J.S. Frank and G.A. Langer. The myocardial interstitium: Its structure and its role in ionic exchange. *Journal of Cell Biology*, 60:596–601, 1974.

[13] Y.C. Fung. Mathematical representation of the mechanical properties of the heart muscle. *Journal of Biomechanics*, 3:381–404, 1970.

[14] K. Sakakura, M. Nakano, F. Otsuka, E. Ladich, F.D Kolodgie, and R. Virmani. Pathophysiology of atherosclerosis plaque progression. *Heart, Lung and Circulation*, 22(6):399–411, 2013.

[15] G. A. Holzapfel, M. Stadler, and C.A.J. Schulze-Bauer. A layer-specific three-dimensional model for the simulation of balloon angioplasty using magnetic resonance imaging and mechanical testing. *Annals of Biomedical Engineering*, 30(6):753–767, 2002.

[16] M.G. Lawlor, M.R. O'Donnell, B.M. O'Connell, and M.T Walsh. Experimental determination of circumferential properties of fresh carotid artery plaques. *Journal of Biomechanics*, 44(9):1709–1715, 2011.

[17] E. Maher, A. Creane, S. Sultan, N. Hynes, C. Lally, and D.J. Kelly. Tensile and compressive properties of fresh human carotid atherosclerotic plaques. *Journal of Biomechanics*, 59(4):613–621, 1996.

[18] G. Holzapfel, G. Sommer, and P. Regitnig. Anisotropic mechanical properties of tissue components in human atherosclerotic plaques. *Journal of Biomechanical Engineering*, 126:657–665, 2004.

[19] D. Balzani, S. Brinkhues, and G. Holzapfel. Constitutive framework for the modeling of damage in collagenous soft tissues with application to arterial walls. *Computer Methods in Applied Mechanics and Engineering*, pages 139–151, 2011.

[20] C.K. Chai, A.C. Akyildiz, L. Speelman, F.J. Gijsen, C.W. Oomens, M.R. van Sambeek, A. van der Lugt, and F.P. Baaijens. Local axial compressive mechanical properties of human carotid atherosclerotic plaques/characterisation by indentation test and inverse finite element analysis. *Journal of Biomechanics*, 46(10):1759–1766, 2013.

[21] H.M. Loree, R.D. Kamm, R.G. Stringfellow, and R.T. Lee. Effects of fibrous cap thickness on peak circumferential stress in model atherosclerotic vessels. *Circulation Research*, 71:850–858, 1992.

[22] D. Tang, C. Yang, S. Mondal, F. Liu, G. Canton, T. Hatsukami, and C. Yuan. A negative correlation between human carotid atherosclerotic plaque progression and plaque wall stress: in vivo mri-based 2d/3d fsi models. *J. of Biomechanics*, 41(4):727–736, 2008.

[23] J. Geng, K.B.C. Tan, and G. Liu. Application of finite element analysis in implant dentistry: a review of the literature. *Journal of Prosthetic Dentistry*, 85:585–598, 2001.

[24] R.M. Pilliar, D.A. Deporter, P.A. Watson, and N. Valiquette. Dental implant design/effect on bone remodeling. *Journal of Biomedical Materials Research*, 25(4):467–483, 1991.

[25] H. Vaillancourt, R.M. Pillar, and D. McCammond. Factors affecting crestal bone loss with dental implants partially covered with a porous coating: a finite element analysis. *International Journal of Oral & Maxillofac Implants*, 11(3):351–359, 1996.

[26] O. Dilek, E. Tezulas, and M. Dincel. Required minimum primary stability and torque values for immediate loading of mini dental implants: an experimental study in nonviable bovine femoral bone. *Oral Surgery, Oral Medicine, Oral Pathology, Oral Radiology, and Endodontology*, 105(2):20–27, 2008.

[27] M. Chaiapasco, S. Abati, E. Romeo, and G. Vogel. Implant/retained mandibular overdentures with Branemark system MKII implants: a prospective comparative study between delayed and and immediate loading. *International Journal of Oral & Maxillofac Implants*, 16(4):537–546, 2001.

[28] O. Kayabasi, E. Yuzbasioglu, and F. Erzincanli. Static, dynamic and fatigue behaviors of dental implant using finite element method. *Advances in Engineering Software*, 37:649–658, 2006.

[29] G. E. Wider, J. A. Tesk, and E. Privitzer. Interaction effects among cortical bone, cancellous bone, and periodontal membrane of natural teeth and implants. *Journal of Biomedical Matererials Research*, 10(4):613–623, 1976.

[30] H. Van Oosterwyck, J. Duyck, J. Vander Sloten, G. Van der Perre, M. De Cooman, S. Lievens, R. Puers, and I. Naert. The influence of bone mechanical properties and implant fixation upon bone loading around oral implants. *Clinical Oral Implants Research*, 36:1017–1043, 1998.

[31] L. Formaggia, J.F. Gerbeau, F. Nobile, and A. Quarteroni. On the coupling of 3D and 1D Navier-Stokes equations for flow problems in compliant vessels. *Computer Methods in Applied Mechanics and Engineering*, 191(6-7):561–582, 2001.

[32] E Carrera. Theories and finite elements for multilayered plates and shells: a unified compact formulation with numerical assessment and benchmarking. *Archives of Computational Methods in Engineering*, 10(3):215–296, 2003.

[33] E. Carrera and G. Giunta. Refined beam theories based on Carreras unified formulation. *International Journal of Applied Mechanics*, 2(1):117–143, 2010.

[34] E. Carrera, M. Cinefra, M. Petrolo, and E. Zappino. *Finite Element Analysis of Structures through Unified Formulation*. John Wiley & Sons, Chichester, West Sussex, UK., 2014.

[35] E. Carrera, M. Maiarú, and M. Petrolo. Component-wise analysis of laminated anisotropic composites. *International Journal of Solids and Structures*, 49:1839–1851, 2012.

[36] E. Carrera, M. Maiarú, M. Petrolo, and G. Giunta. A refined 1D element for the structural analysis of single and multiple fiber/matrix cells. *Composite Structures*, 96:455–468, 2013.

[37] E. Carrera, A. Pagani, and M. Petrolo. Classical, refined and component-wise theories for static analysis of reinforced-shell wing structures. *AIAA Journal*, 51(5):1255–1268, 2013.

[38] E. Carrera and A. Pagani. Free vibration analysis of civil engineering structures by component-wise models. *Journal of Sound and Vibration*, 333(19):4597–4620, 2014.

[39] E. Carrera and M. Filippi. Variable kinematic one-dimensional finite elements for the analysis of rotors made of composite materials. *Journal of Engineering for Gas Turbines and Power*, 136(9), 2014. doi: 10.1115/1.4027192.

[40] E. Zappino, E. Carrera, S. Rowe, C. Mangeot, and H. Marques. Numerical analyses of piezoceramic actuators for high temperature applications. *Composite Structures*, 151:36–46, 2016.

[41] E. Carrera, A. Pagani, M. Petrolo, and E. Zappino. Recent developments on refined theories for beams with applications. *Mechanical Engineering Reviews*, 2(2):1–30, 2015.

[42] A. Varello and E. Carrera. Nonhomogeneous atherosclerotic plaque analysis via enhanced 1D structural models. *Smart Structures and Systems*, 13(4):659–683, 2014.

[43] M. Petrolo E. Carrera, G. Giunta. *Beam structures: classical and advanced theories*. John Wiley and Sons, 2011.

[44] A. Pagani, M. Boscolo, J. R. Banerjee, and E. Carrera. Exact dynamic stiffness elements based on one-dimensional higher-order theories for free vibration analysis of solid and thin-walled structures. *Journal of Sound and Vibration*, 332(23):6104–6127, 2013.

[45] E. Carrera and M. Petrolo. Refined beam elements with only displacement variables and plate/shell capabilities. *Meccanica*, 47(3):537–556, 2012.

[46] E. Carrera, A. Pagani, and M. Petrolo. Component-wise method applied to vibration of wing structures. *Journal of Applied Mechanics*, 80(4):art. no. 041012 1–15, 2013.

[47] E. Carrera, A.G. de Miguel, and A. Pagani. Hierarchical theories of structures based on Legendre polynomial expansions with finite element applications. *International Journal of Mechanical Sciences*, 120:286–300, jan 2017.

[48] A. Pagani, A.G. de Miguel, M. Petrolo, and E. Carrera. Analysis of laminated beams via unified formulation and Legendre polynomial expansions. *Composite Structures*, 156:78–92, nov 2016.

[49] E. Carrera and E. Zappino. One-dimensional finite element formulation with node-dependent kinematics. 2017. Submitted.

[50] E. Carrera, A. Pagani, and M. Petrolo. Classical, refined and component-wise theories for static analysis of reinforced-shell wing structures. *AIAA Journal*, 51(5):1255–1268, 2013.

[51] E. Carrera, A. Pagani, and M. Petrolo. Refined 1D finite elements for the analysis of secondary, primary, and complete civil engineering structures. *Journal of Structural Engineering*, 141(4):art. no. 04014123, 2014.

[52] R. J. Allemang and D. L. Brown. A correlation coefficient for modal vector analysis. In *Proceedings of the International Modal Analysis Conference*, pages 110–116, Orlando, Florida, USA, 1982.